Global Biogeochemical Cycles

RESEARCH ARTICLE
10.1029/2023GB007696

Underestimated Interannual Variability of Terrestrial Vegetation Production by Terrestrial Ecosystem Models

Shangrong Lin[1,2], Zhongmin Hu[2,3], Yingping Wang[4], Xiuzhi Chen[1,2], Bin He[5], Zhaoliang Song[6], Shaobo Sun[6], Chaoyang Wu[7], Yi Zheng[1,2], Xiaosheng Xia[1], Liyang Liu[8], Jing Tang[9,10], Qing Sun[11], Fortunat Joos[11], and Wenping Yuan[1,2]

[1]School of Atmospheric Sciences, Guangdong Province Data Center of Terrestrial and Marine Ecosystems Carbon Cycle, Sun Yat-sen University, Zhuhai, China, [2]Southern Marine Science and Engineering Guangdong Laboratory (Zhuhai), Guangdong, China, [3]College of Ecology and Environment, Hainan University, Haikou, China, [4]CSIRO, Oceans and Atmosphere, Aspendale, VIC, Australia, [5]College of Global Change and Earth System Science, Beijing Normal University, Beijing, China, [6]Institute of Surface-Earth System Science, School of Earth System Science, Tianjin University, Tianjin, China, [7]The Key Laboratory of Land Surface Pattern and Simulation, Institute of Geographical Sciences and Natural Resources Research, Chinese Academy of Sciences, Beijing, China, [8]Laboratoire des Sciences du Climat et de l'Environnement, IPSL, CEA-CNRS-UVSQ, Université Paris-Saclay, Gif-sur-Yvette, France, [9]Department of Physical Geography and Ecosystem Science, Lund University, Lund, Sweden, [10]Department of Biology, University of Copenhagen, Copenhagen, Denmark, [11]Climate and Environmental Physics, Physics Institute, University of Bern, Bern, Switzerland

Abstract Vegetation gross primary production (GPP) is the largest terrestrial carbon flux and plays an important role in regulating the carbon sink. Current terrestrial ecosystem models (TEMs) are indispensable tools for evaluating and predicting GPP. However, to which degree the TEMs can capture the interannual variability (IAV) of GPP remains unclear. With large data sets of remote sensing, in situ observations, and predictions of TEMs at a global scale, this study found that the current TEMs substantially underestimate the GPP IAV in comparison to observations at global flux towers. Our results also showed the larger underestimations of IAV in GPP at nonforest ecosystem types than forest types, especially in arid and semiarid grassland and shrubland. One cause of the underestimation is that the IAV in GPP predicted by models is strongly dependent on canopy structure, that is, leaf area index (LAI), and the models underestimate the changes of canopy physiology responding to climate change. On the other hand, the simulated interannual variations of LAI are much less than the observed. Our results highlight the importance of improving TEMs by precisely characterizing the contribution of canopy physiological changes on the IAV in GPP and of clarifying the reason for the underestimated IAV in LAI. With these efforts, it may be possible to accurately predict the IAV in GPP and the stability of the global carbon sink in the context of global climate change.

Key Points:

- Current terrestrial ecosystem models (TEMs) substantially underestimate the interannual variability (IAV) of gross primary production (GPP) in comparison to observations at global flux sites
- The IAV of GPP in TEMs is strongly depended on leaf area index (LAI), which is one of the causes for the underestimation of IAV in GPP and the simulated IAV in LAI from TEMs is much less than the observation
- Precisely characterizing the contribution of vegetation physiological changes may improve the performance of predicting IAV in GPP from TEMs

Supporting Information:

Supporting Information may be found in the online version of this article.

Correspondence to:

W. Yuan,
yuanwp3@mail.sysu.edu.cn

Citation:

Lin, S., Hu, Z., Wang, Y., Chen, X., He, B., Song, Z., et al. (2023). Underestimated interannual variability of terrestrial vegetation production by terrestrial ecosystem models. *Global Biogeochemical Cycles*, *37*, e2023GB007696. https://doi.org/10.1029/2023GB007696

Received 11 JAN 2023
Accepted 20 MAR 2023

Author Contributions:

Conceptualization: Shangrong Lin, Zhongmin Hu, Yingping Wang, Wenping Yuan

1. Introduction

Terrestrial vegetation production is a critical component of the global carbon cycle and plays an important role in regulating terrestrial carbon sinks (Beer et al., 2010; Jung et al., 2017). In particular, interannual variability (IAV) in vegetation production substantially regulates terrestrial carbon sinks (Desai et al., 2010), atmospheric CO_2 concentration (Yuan et al., 2019), and the climate system (Poulter et al., 2014). For example, previous studies indicated that the IAV in global gross vegetation production strongly correlates with IAV in atmospheric CO_2 concentration (Reichstein et al., 2013). With the rising frequency of extreme climate events, vegetation production shows an increasing interannual fluctuation (Reichstein et al., 2013; Zscheischler, Mahecha, et al., 2014; Zscheischler, Michalak, et al., 2014), which also indicates a decreasing stability of ecosystem carbon sinks (Messori et al., 2019; Zscheischler, Mahecha, et al., 2014; Zscheischler, Michalak, et al., 2014). With more frequent climate extremes under climate change (Seneviratne et al., 2012), the impact of IAV in gross primary production (GPP) is likely to increase (Reichstein et al., 2013). Thus, a better understanding of the performance of modeled IAV in GPP will help inferring how carbon sinks and sources will change across regions in the future (Z. Li et al., 2020; Poulter et al., 2014).

Terrestrial ecosystem models (TEMs) are an irreplaceable tool for estimating and predicting the terrestrial carbon sink and its IAV (Friedlingstein et al., 2020). However, there are substantial differences in the simulated IAV in gross vegetation production from various ecosystem models (Cai et al., 2014; M. Chen et al., 2017). For example, a recent study showed large differences of IAV (characterized by the standard deviation in annual GPP,

Data curation: Bin He, Yi Zheng, Xiaosheng Xia, Liyang Liu, Jing Tang, Qing Sun
Funding acquisition: Wenping Yuan
Investigation: Bin He
Methodology: Shangrong Lin
Supervision: Zhaoliang Song, Chaoyang Wu, Wenping Yuan
Validation: Shangrong Lin
Writing – original draft: Shangrong Lin, Zhongmin Hu, Yingping Wang, Xiuzhi Chen, Shaobo Sun, Wenping Yuan
Writing – review & editing: Shangrong Lin, Zhongmin Hu, Wenping Yuan

ranging from 1.38 to 5.89 Pg C yr^{-1}) in simulated GPP over 11 TEMs (Zheng et al., 2020). Similarly, O'Sullivan et al. (2020) found that the global average variance of IAV in GPP simulated by TEMs is almost 1.21 Pg C yr^{-1}, which is larger than the one obtained from satellite-based models (1.01 Pg C yr^{-1}) and machine-learning models (0.34 Pg C yr^{-1}). In addition, when tested against site-based observations in terms of IAV in GPP, TEMs typically perform very poorly (Keenan et al., 2012; Verma et al., 2015). For example, Keenan et al. (2012) tested 16 TEMs and three remote sensing products against the measurements at 11 long-term eddy covariance sites and found that none of the models reproduced the observed IAV in GPP. Therefore, Earth System Models, which have integrated the TEMs, may induce large uncertainties for reproducing IAV of gross vegetation production as well as the terrestrial carbon cycle in the future (Bonan & Doney, 2018; Winkler et al., 2019).

Simulated IAV in GPP remains highly uncertain and is related to the poor representation of model formulation (Dietze et al., 2011). In general, the simulated IAV in GPP derived from TEMs highly depends on two sources, including (a) changes in physiological processes such as growing season length, and photosynthesis rates (X. Luo et al., 2019; MacBean et al., 2018; Xia et al., 2015; Zscheischler et al., 2016) and (b) changes in vegetation structural variable, that is, leaf area index (J. M. Chen et al., 2019; S. Chen et al., 2019; Hu et al., 2018). Although most of the key carbon cycle processes have been integrated into models, there are large challenges in reproducing IAV in GPP because of the complicated processes and responses to environmental variables (Verma et al., 2015; Zheng et al., 2020). The physiological responses of vegetation to environmental changes are instantaneous (Liu et al., 2021; X. Luo et al., 2019; Zscheischler et al., 2016), but the structural responses are lagged (Bastos et al., 2020; Bertrand et al., 2011; A. Zhao et al., 2020; Q. Zhao et al., 2020). For example, although the canopy structure of Amazon forests shows slight changes over the years, the photosynthetic rate largely differs across years (Saleska et al., 2016; Wu et al., 2017). Magney et al. (2019) showed similar results in temperate forests. The understanding of the differential changes in physiology and structure in anomalous climate conditions have not yet been applied to improve model predictive skills (Hu et al., 2018), which may be the main cause for the low predictive skills for reproducing IAV in GPP.

This study aims to evaluate the performance of TEMs for reproducing IAV in GPP against observations at eddy covariance towers globally and to investigate the relationships of IAV in GPP with meteorological variables and leaf area index to understand its environmental and physiological controls. Specific objectives are to (a) evaluate the modeling capabilities of TEMs for simulating IAV in GPP based on global observations, (b) examine the performance of TEMs for reproducing vegetation structural changes, and (c) quantify the impacts of vegetation physiological and structural changes on IAV in GPP.

2. Materials and Methods

2.1. Terrestrial Ecosystem Models

This study included nine TEM data sets from the TRENDY v10 ensemble since 2000 (Friedlingstein et al., 2022): Community Atmosphere Biosphere Land Exchange (CABLE-POP, Haverd et al., 2017, hereafter CABLEP), Community Land Model (CLM, Lawrence et al., 2019), Dynamic Land Ecosystem Model (DLEM, Tian et al., 2015), Interactions between Surface, Biosphere, and Atmosphere (IBSA, Delire et al., 2020), Integrated BIosphere Simulator (IBIS, Yuan et al., 2014), Lund-Potsdam-Jena General Ecosystem Simulator (LPJ-GUESS, Smith et al., 2014, hereafter LPJG), Land surface Processes and eXchanges (LPX, Lienert & Joos, 2018), Organizing Carbon and Hydrology in Dynamic Ecosystems (ORCHIDEEv3, Vuichard et al., 2019, hereafter ORCHIDEE), and Vegetation Integrated Simulator for Trace gases (VISIT, Kato et al., 2013). We used the simulations in model experiments with varying CO_2 concentrations and climate (i.e., S2 experiment), which are close to the scenarios in the real world. The simulation in S2 experiment considers variability in CO_2 and climate, with the assumption that land cover type is stable compared to S3 experiment (Friedlingstein et al., 2022). All TEMs from the TRENDY v10 were driven by CRUJRA data set with a coarse spatial resolution of 0.5° × 0.5° (see Section 2.2). In addition, we run four TEMs (i.e., IBIS, LPJG, LPX, and ORCHIDEE) driven by site-based meteorological measurements to investigate whether the coarse spatial resolution of climate forcing impacted the model performance when reproducing IAV in GPP.

The annual GPP and LAI were averaged from monthly simulations during the growing season. This study defined the growing season at those months with a mean temperature was above 0°C based on the Climatic Research Unit Japanese Reanalysis (CRU-JRA, http://catalogue.ceda.ac.uk/uuid/863a47a6d8414b6982e1396c69a9efe8)

Table 1
Investigated Sites in This Study (Detailed Site Information Could Be Found in Table S1 in Supporting Information S1)

	Sites	Site-years	Mean annual temperature (°C)	Mean annual precipitation (mm)
ENF	53	457	−3.2–14.2	523–1,316
EBF	15	103	10.7–26.1	650–4,000
DBF	27	228	0.3–15.1	563–2,275
MF	12	70	1.3–15.8	408–2,100
SAV	16	141	15.8–21.9	240–1,449
GRA	49	374	−9.7–8.7	93–1,100
SHR	15	106	−14.3–27.2	220–588
CRO	24	207	7.6–18.0	470–1150

Note. We chose eight types of major biomes including evergreen needleleaf forest (ENF), evergreen broadleaf forest (EBF), deciduous broadleaf forest (DBF), mixed forest (MF), savanna (SAV), grassland (GRA), shrub (SHR), and cropland (CRO).

data set. Since the spatial resolution of GPP and LAI varies among models, we resampled all the TEM simulated GPP and LAI into a 0.5° × 0.5° spatial resolution.

2.2. Climate and Satellite Data

The meteorological forcing data in TRENDY v10 ensemble is CRUJRA data set, which is a gridded land surface blend of the CRU and the JRA data sets with a spatial resolution of 0.5° × 0.5°. We chose air temperature (TEMP), shortwave radiation (SW), precipitation (PRE), and vapor pressure deficit (VPD) to examine the responses of GPP to climate change. VPD was calculated based on air temperature and actual vapor pressure derived from this data set (Yuan et al., 2019). All the annual meteorological variables were calculated as the average from only the growing season data.

To compare modeled LAI with observation-based LAI data, we utilized the satellite-based 500-m spatial resolution LAI product Global Land Surface Satellite (GLASS, Liang et al., 2021) based on Moderate-resolution Imaging Spectroradiometer (MODIS) observations. This product is generated with physical inversion techniques using the general regression neural networks (GRNNs) method. The GRNNs are trained with fused reflectance values for each MODIS biome and CYCLOPES LAI products. Research has shown that the GLASS-LAI product is in good agreement with ground measured LAI (Fang et al., 2013; Xiao et al., 2014, 2017; B. Xu et al., 2018). The upscale ground measured LAI also showed that the GLASS-LAI product is more accurate than the other existing LAI product in most biomes, so it can be used as a proxy for annual LAI observations (B. Xu et al., 2018). We aggregated the annual LAI observation as the mean LAI values from GLASS-LAI product during the growing season (defined as months with mean air temperature higher than 0°C).

2.3. Data Set at the Eddy Covariance Sites

The IAV in GPP from eddy covariance (EC) sites observation in FLUXNET 2015 (Pastorello et al., 2020), Integrated Carbon Observation System (ICOS, https://www.icos-cp.eu/data-products/2G60-ZHAK), AmeriFlux (https://ameriflux.lbl.gov/sites/site-search/), OzFlux (https://data.ozflux.org.au/portal/home.jspx), and AsiaFlux (https://db.cger.nies.go.jp/asiafluxdb/), was treated as the observation of IAV in GPP in this study. The annual GPP was aggregated from the daytime partition method (GPP_DT_VUT_REF) derived from month GPP data during the growing season. The effective annual GPP, aggregated with more than 10 months of GPP data with its quality control tag >0.8. We excluded the sites with less than 4 years of effective annual GPP, so a total of 211 EC sites including 1686 site-years data were selected (Table 1 and Table S1 in Supporting Information S1). Eight types of major biomes including evergreen needleleaf forest (ENF), evergreen broadleaf forest (EBF), deciduous broadleaf forest (DBF), mixed forest (MF), savanna (SAV), grassland (GRA), shrub (SHR), and cropland (CRO) were selected to evaluate the IAV in GPP at the sites. All TEMs simulated GPP for each ecosystem type individually within a given 0.5 × 0.5° grid, and we compared the simulations of the corresponding ecosystem types against the GPP derived from EC site measurements.

Since the TEMs in TRENDY v10 ensemble are driven by the coarse spatial resolution climate data, the meteorological conditions may differ from those at the flux sites and lead to uncertainties in the evaluation of IAV in GPP of the models. Therefore, we compared IAV in the site-measured meteorology data (i.e., SW, VPD, PRE and TEMP) with the CRU-JRA data at the selected sites.

2.4. Calculating Interannual Variability

Because the magnitudes of simulated LAI and GPP vary across TEMs (Zhang & Ye, 2021; A. Zhao et al., 2020; Q. Zhao et al., 2020) and have an annual trend, quantitative methods (i.e., anomalies and standard deviations) of IAV used in previous research (M. Chen et al., 2017; O'Sullivan et al., 2020; Yuan et al., 2009) are not applicable to this study. We evaluated the IAV of each variable for each site or grid by calculating the coefficient of variation

(CV) with annual detrended data, which has been found to be an effective measure of IAV (Cao et al., 2003). We used a linear annual detrending method to remove the annual trend from the data:

$$X_{\text{detrend,year}} = X_{\text{year}} - X_{\text{trend,year}} + X_{\text{mean}} \quad (1)$$

$$X_{\text{trend,year}} = k \times \text{year} + b \quad (2)$$

where X_{year} is the original annual variable with annual trend; $X_{\text{trend,year}}$ represents the trend of each year, whose the coefficients (k, b) in Equation 2 are fitted by a linear function with year as input and X_{year} as output. We used X_{mean}, which is averaged from X_{year}, to denote the magnitude of the variable. The detrended variable in each year is represented by $X_{\text{detrend,year}}$. The IAV, indicated by CV, in each variable (CV_x) was calculated from the detrended data:

$$\text{CV}_x = \frac{\sqrt{\frac{\sum \left(X_{\text{detrend,year}} - X_{\text{mean}}\right)^2}{N}}}{X_{\text{mean}}} \quad (3)$$

where N is the total number of investigated years in each site or grid. In different vegetation types and TEMs, the magnitudes of GPP can be quite different (Zhang & Ye, 2021), so using a ratio (i.e., CV) between standard deviation of GPP and average GPP can better quantify the fluctuation of GPP over many years across regions and models (Dong et al., 2022).

2.5. Evaluating the Relationship Between Structural Changes and GPP

To evaluate how the structural changes (i.e., LAI) affect GPP, we used 211 FLUXNET sites locations to extract the annual LAI and GPP from both observed and simulated data. To estimate the influence of annual structural change to GPP, we derived the correlation (indicated by Pearson's correlation coefficient, r) between annual detrended LAI and annual aggregated GPP at each EC site. To assess the spatial pattern of IAV of LAI to GPP, we used a linear fitting method to compare CV in LAI versus CV in GPP at the EC sites. We derived CV in GLASS-LAI as observation and CV in TEMs' LAI as simulation to compare the discrepancy in the IAV in LAI at a global scale.

2.6. Separating Contributions of Structural and Physiological Changes on IAV in GPP

A machine learning model based on random forest (RF) was used to quantify the contributions of vegetation physiological and structural changes on IAV in GPP. First, we developed an RF model to reproduce IAV in GPP derived from TEMs and observed GPP at EC sites, which included the impacts of physiological and structural changes in vegetation. This study defined the structural change of vegetation as the LAI changes, and thus the contribution of structural changes to IAV in GPP is the contribution of LAI changes with other environmental variables remaining constant. The contribution of physiological changes to IAV in GPP was quantified as the impacts of meteorological variables (Peng et al., 2021; Wu et al., 2017; Zscheischler et al., 2016). We included four meteorological variables (annual mean air temperature, vapor pressure deficit, shortwave radiation and annual total precipitation) to quantify the contributions of physiological changes. To avoid the impacts of long-term changes on IAV, we used detrended meteorological variables, LAI and GPP, to develop the RF model using the "randomForest" package in R modified by Liaw and Wiener (2002). We constructed the RF model at each EC site and each pixel and randomly chose 70% of the data for training and the remaining 30% of the data for validation, and repeated this process 200 times. The simulated GPP by the RF model (GPP_{ALL}) were the mean values of all validated data in each year.

Next, to quantify the contributions of physiological and structural changes to IAV in GPP, we conducted two model experiments by holding meteorological variables and LAI constant to simulate GPP, indicated as GPP_{MET0} and GPP_{LAI0}, respectively. The contributions of physiological and structural changes to IAV in GPP were calculated as follows:

$$\text{Con}_{\text{P}} = \frac{(\text{MSE}_{\text{LAI0}} - \text{MSE}_{\text{ALL}})}{\text{MSE}_{\text{ALL}}} \times 100\% \quad (4)$$

$$\text{MSE}_{\text{ALL}} = \frac{\sum (\text{GPP}_{\text{ALL}} - \text{GPP}_{\text{ORI}})^2}{N} \quad (5)$$

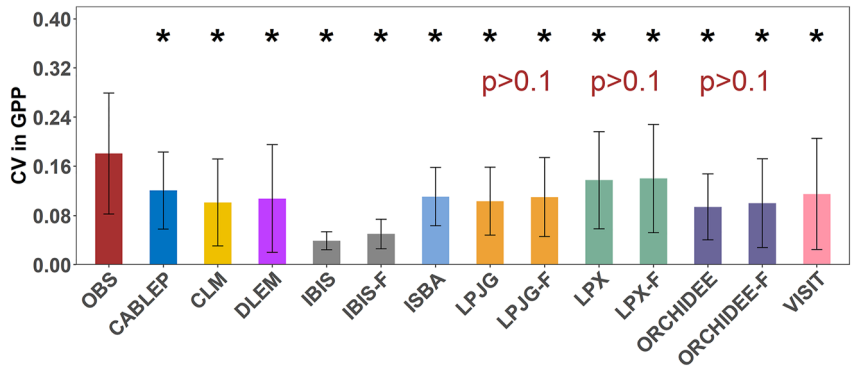

Figure 1. Comparison of the coefficient of variation of observed and simulated gross primary production (GPP) averaged from 211 eddy covariance sites. The asterisks (*) indicate statistically significant differences ($p < 0.05$) between observations (OBS) and simulations. The error bars represent the standard deviation in each model. The series of IBIS-F, LPJG-F, LPX-F, and ORCHIDEE-F indicated the interannual variability (IAV) in GPP driven by site-based meteorology data. The *p*-value in red color represented the paired *t*-test between IAV in GPP from TRENDY v10 ensemble and IAV in GPP driven by site-based meteorology data.

$$\mathrm{MSE}_{\mathrm{LAI0}} = \frac{\sum (\mathrm{GPP}_{\mathrm{LAI0}} - \mathrm{GPP}_{\mathrm{ORI}})^2}{N} \quad (6)$$

where $\mathrm{GPP}_{\mathrm{ALL}}$ is the simulated GPP by the RF model driven by changing meteorological variables and LAI with time; $\mathrm{GPP}_{\mathrm{ORI}}$ is the observed GPP at EC sites or simulated GPP by nine TEMs; $\mathrm{Con}_{\mathrm{P}}$ indicates the contribution of physiological changes to IAV in GPP. The contribution of structural changes ($\mathrm{Con}_{\mathrm{S}}$) can be calculated by replacing $\mathrm{GPP}_{\mathrm{LAI0}}$ to $\mathrm{GPP}_{\mathrm{MET0}}$ in Equations 4 and 6. According to the above methods, we calculated the $\mathrm{Con}_{\mathrm{P}}$ and $\mathrm{Con}_{\mathrm{S}}$ at the site level and global scale based on nine terrestrial models from 2000 to 2020. Both $\mathrm{Con}_{\mathrm{P}}$ and $\mathrm{Con}_{\mathrm{S}}$ are affected by the magnitude of the input variables and GPP models; therefore, we calculated the relative contribution ratio from $\mathrm{Con}_{\mathrm{P}}$ divided by $\mathrm{Con}_{\mathrm{S}}$ to characterize the principal driver (i.e., physiological or structural change) of IAV in GPP from observations and simulations.

3. Results

3.1. IAV in GPP From TEMs

The TEMs underestimated the IAV (indicated by the coefficient of variation, CV) in GPP against the observations at eddy covariance (EC) sites. The mean CV values of simulated annual GPP by nine TEMs from TRENDY data set ranged from 0.04 to 0.15, all of which were significantly lower than the mean CV in the observed GPP (i.e., 0.18) (Figure 1). The GPP simulations by four TEMs (i.e., IBIS, LPJG, LPX, and ORCHIDEE), driven by site-based meteorology measurements, also showed a significant underestimation compared with the IAV in GPP observed from EC sites. In addition, both observations and simulations showed that the CV in GPP steadily decreased logarithmically with mean annual precipitation, suggesting that the IAV in GPP was larger in drier ecosystems ($p < 0.05$, Figure 2).

Further, we examine the model performance for simulating IAV in GPP for various ecosystem types and geographical regions. At nearly all ecosystem types, almost all TEMs underestimated the IAV in GPP compared with the IAV in observed GPP (Figure 3). The CV differences, defined as CV in simulated GPP minus CV in observed GPP, indicated significantly lower CV values of simulated GPP than those of observed GPP across almost all ecosystem types (Figure 3). The results showed the larger underestimates of CV in GPP by TEMs at nonforest ecosystem types (i.e., SAV, GRA, SHR, CRO) than four forest types (Figure S1 in Supporting Information S1). In

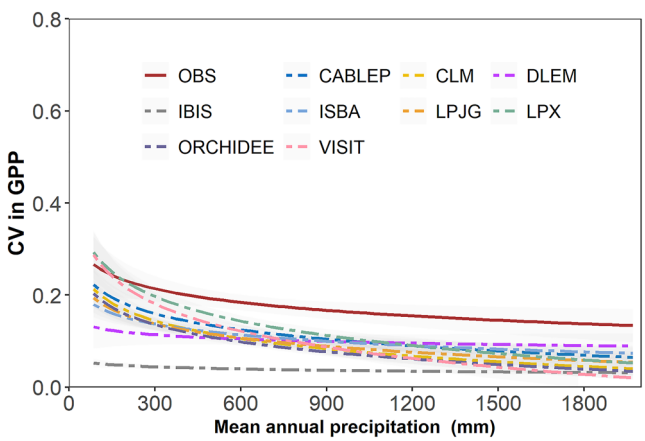

Figure 2. Spatial patterns of interannual variations in gross primary production (GPP) over 211 eddy covariance sites along the mean annual precipitation gradient. The solid line indicates the regression line of observed GPP (OBS) based on the eddy covariance measurements, and the other dashed lines indicate the regression lines of simulations by nine terrestrial ecosystem models. All the regression correlation is significant with $p < 0.05$.

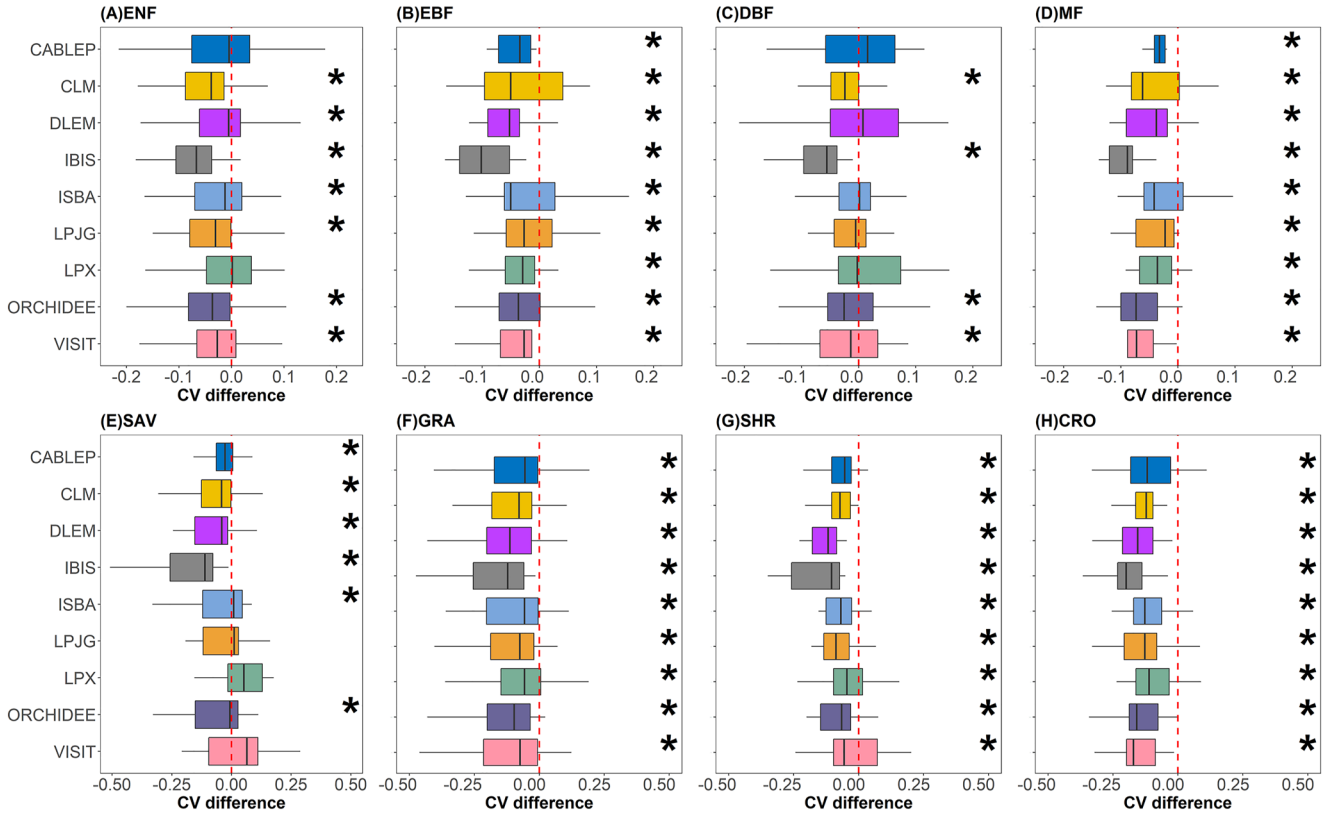

Figure 3. Difference of coefficient of variation (CV) in gross primary production between simulations and observations at eight vegetation types. The red dashed line in the middle represents the CV difference equals to zero. The asterisks (*) indicate statistically significant differences ($p < 0.05$) between simulated CV and observed CV. The abbreviations of each subplot: ENF, evergreen needleleaf forest; EBF, evergreen broadleaf forest; DBF, deciduous broadleaf forest; MF, mixed forest; SAV, savanna; GRA, grassland; SHR, shrubland; and CRO, cropland.

addition, the results also found that the TEMs underestimated the IAV in GPP at various geographical regions including Asia, Oceania, Europe, North America, South America, Northern Hemisphere, and Southern Hemisphere (Figure S3 in Supporting Information S1).

3.2. IAV in GPP Depends on IAV in LAI in TEMs

To investigate the reason for the underestimations of IAV by TEMs, we first examined the how variance of vegetation structure affects annual GPP. Our results showed that the models overestimated the dependence of GPP on LAI. On average, over all investigated sites, the correlation coefficient (r) between simulated annual LAI and annual GPP ranges from 0.60 to 0.95 for seven models (Figure 4a) except for LPJG and LPX. On the contrary, the averaged r between satellite-based LAI and observed GPP was only 0.13. In general, larger IAV in LAI simulations led to higher IAV in GPP (Figure 4b). However, the observed IAV in GPP had a weak correlation ($r = 0.2$) with IAV in LAI over all investigated sites (Figure 4b). The simulated IAV in GPP derived from most models are significantly and positively correlated with LAI at more than 50% of the EC sites (Figure 4c) except for LPJG and LPX. In comparison, the CV of the observed GPP showed weak correlations with LAI. Only at 13% of the sites, the satellite-based LAI showed a significant correlation to IAV in the observed GPP (Figure 4c). In addition, the strong correlations between simulated GPP and LAI by nine TEMs were also found at the global scale (Figure 5).

To distinguish which biome's IAV in GPP is more dependent on IAV in LAI, we compared the annual LAI and GPP at each site across eight major biomes (Figure 6). The site observation data showed that the correlation (r) between annual LAI and annual GPP was weak (~0.2) at most biomes. However, most TEMs showed high correlation ($r > 0.5$) between annual LAI and annual GPP at all biomes, expect for IBIS, LPJG, and LPX.

The TEMs show the strong dependence of IAV in GPP on LAI (i.e., structural variation), but they underestimate the IAV in LAI compared to satellite-based LAI derived from the GLASS-LAI data set (Figure 7), which may

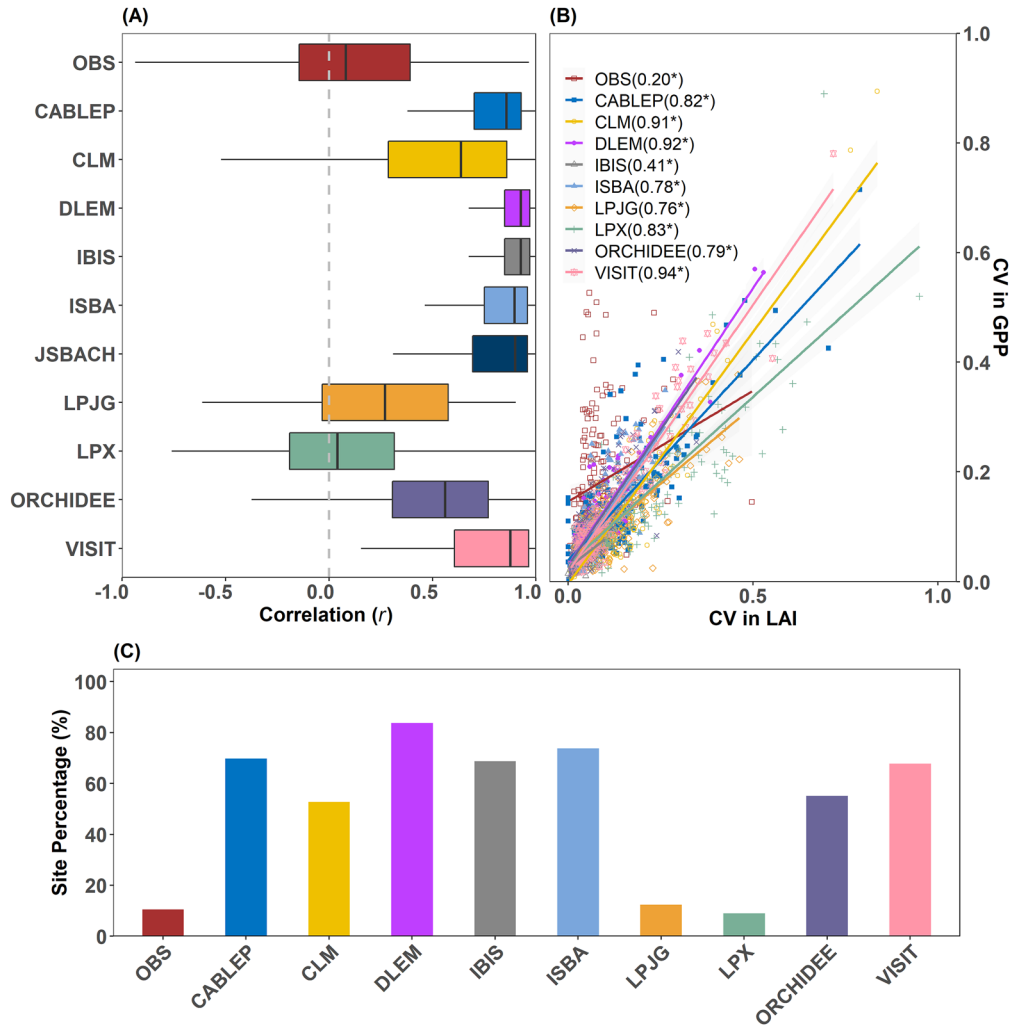

Figure 4. Comparison of correlations of interannual variability in gross primary production (GPP) and leaf area index (LAI) at 211 eddy covariance sites. (a) Boxplot of correlation coefficient (r) between annual GPP and annual LAI. OBS indicates the correlations of observed GPP and satellite-based LAI. The correlations of nine models were calculated between GPP and LAI simulations by model. (b) Correlations of coefficient of variation (CV) in GPP and CV in LAI derived from observations and simulations. The numbers between parentheses show the correlation coefficients r; asterisks represent the statistical significance of $p < 0.05$. Each dot represents the CV in LAI and CV in GPP at a FLUXNET site location. (c) The proportion of sites with significant ($p < 0.05$) correlations between annual LAI and annual GPP within the 211 EC sites.

be one of the most important reasons for underestimating IAV in GPP by TEMs. The global mean satellite-based CV of LAI was 0.23, which was much higher than the CV of simulated LAI by nine TEMs (Figure 7). GLASS-LAI reached its maximal global area proportion when its CV in LAI equals to 0.14. On contrary, the peaks of CV in the simulated LAI by TEMs were much lower; only the ISBA and LPJG showed their largest global area proportion at a CV in LAI around 0.06, while other models did not show the available peak of CV in the simulated LAI (Figure 7).

3.3. Contribution of Physiological Changes to IAV in GPP

This study further compared the relative contribution of physiological changes (Con_P) and structural changes (Con_S) to IAV in GPP. Both Con_p and Con_s depended on the magnitude of GPP; therefore, the absolute values of Con_p and Con_s were not comparable due to different magnitudes of observed and simulated GPP. Thus, the contribution ratio between Con_p and Con_s was calculated to indicate the relative contribution of physiological and structural changes. The contribution ratio derived from observations at 211 EC sites was 5.3, suggesting that

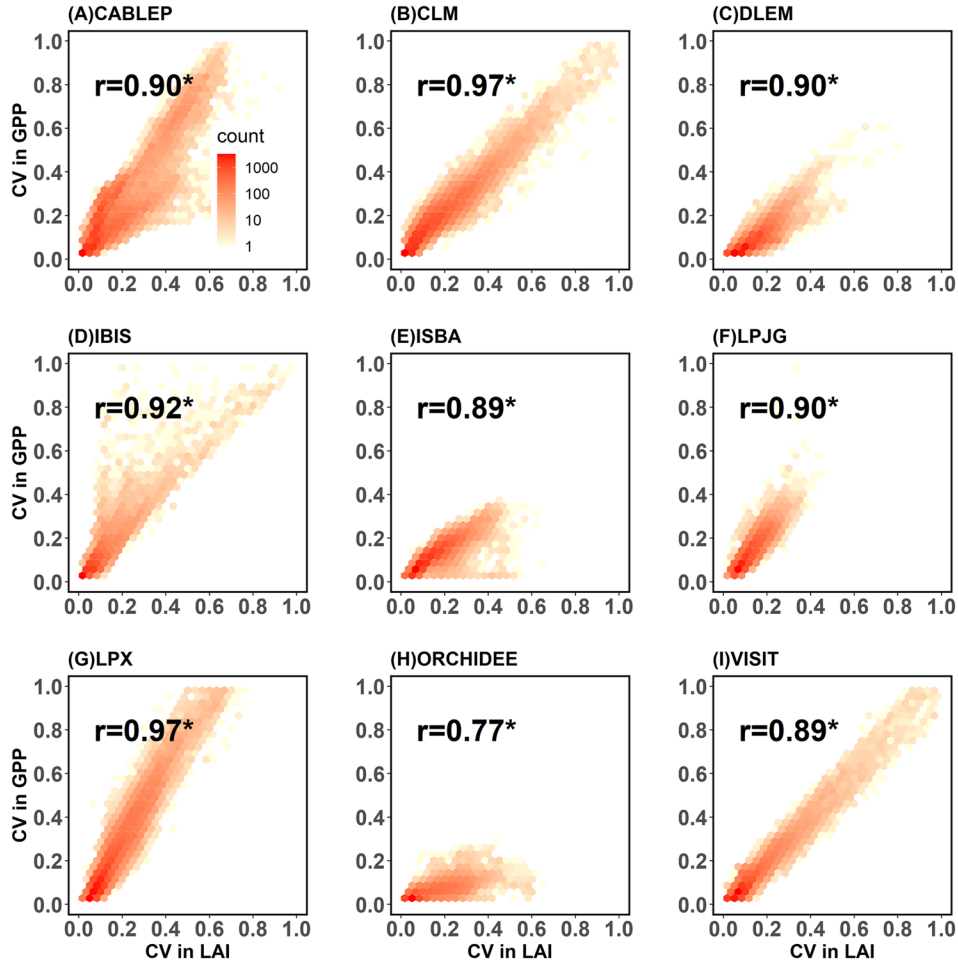

Figure 5. Density plots of correlations between coefficient of variation (CV) in leaf area index and CV in gross primary production over global vegetated pixels in terrestrial ecosystem models. Correlation coefficient (r) with an asterisk represents $p < 0.05$.

the contribution of physiological changes to IAV in GPP was five times that of structural changes (Figure 8a). However, the contribution ratios derived from simulations from TEMs ranged from 2.7 to 4.9, which were significantly lower than the observations (i.e., 5.3) expect for LPJG and LPX. Among these models, only LPJG and LPX predicted large contribution ratios (i.e., 5.1 and 5.4), which were close to the ratio derived from observations. Similarly, at the global scale, all models showed a similar contribution ratio to those at the EC sites (Figure 8b).

4. Discussions

4.1. Underestimation of GPP Interannual Variability by TEMs and Its Causes

We found that most TEMs underestimated the IAV in GPP. Other lines of evidence support our conclusion (Stocker et al., 2019; Zhang et al., 2019). For example, Zhang et al. (2019) demonstrated the low sensitivity of TEMs to climate change, resulting in underestimates of the effect of El Niño/Southern Oscillation on global GPP. Considering that IAV in GPP explained a significant proportion of IAV in the magnitude of net ecosystem production (NEP) (Yuan et al., 2009), the underestimation of IAV in GPP may result in overestimating the stability of the terrestrial carbon sink. More importantly, the terrestrial carbon sink substantially controls the interannual variations in atmospheric CO_2 growth rates (He et al., 2021). Therefore, underestimating IAV in GPP may also potentially result in underestimating the IAV in atmospheric CO_2.

Our results suggest that the overestimated coupling between LAI and GPP, in combination with underestimated IAV in LAI, caused the underestimation of GPP variability by the models (Figures 4–7). Simulated high coupling

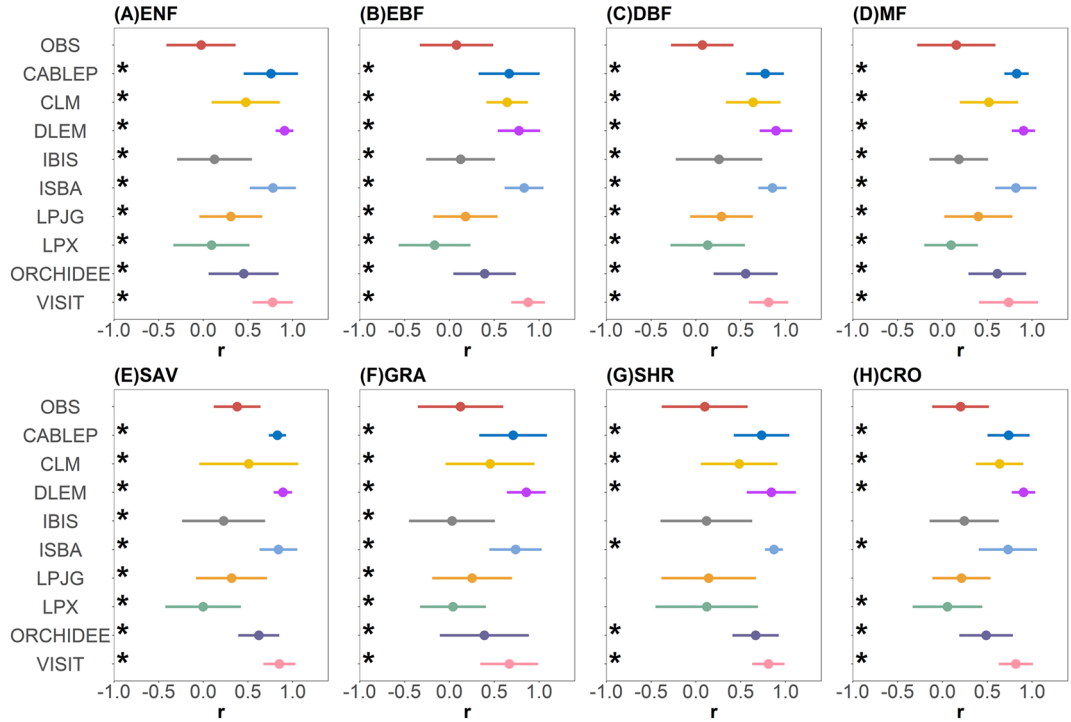

Figure 6. The relationship between annual leaf area index and annual gross primary production at site level among biomes derived from flux site observations (OBS) and simulations (TRENDY v10 ensemble). The asterisks represent the statistical significance of $p < 0.05$ between model simulations and observations. The abbreviations of each subplot: ENF, evergreen needleleaf forest; EBF, evergreen broadleaf forest; DBF, deciduous broadleaf forest; MF, mixed forest; SAV, savanna; GRA, grassland; SHR, shrubland; and CRO, cropland.

between LAI and GPP by models has been reported in previous research ((J. M. Chen et al., 2019; S. Chen et al., 2019; Higuchi et al., 2005; Wang et al., 2011). However, our finding is consistent with observations showing that vegetation structure (i.e., LAI) has limited impacts compared to physiological changes (Hu et al., 2018; Liu et al., 2021; Walther et al., 2016). Studies suggested that intra-seasonal changes in meteorological conditions can significantly affect plant leaf photosynthesis but not LAI, which, consequenctly affects the annual amount of GPP (Zscheischler et al., 2016). For example, Doughty et al. (2019) found that a physiological change indicator, solar induced fluorescence, detected a decrease in GPP during drought years and seasons; however, LAI and vegetation index have a limited response to such conditions (X. Li & Xiao, 2020). In addition, meteorological conditions often exhibit time-lag effects on canopy structure, which might be another reason for the decoupling between GPP and LAI (Bertrand et al., 2011; Mulder et al., 2017; Sherry et al., 2008). However, few models can reproduce the time-lag effects observed in terrestrial ecosystems (Wen et al., 2019).

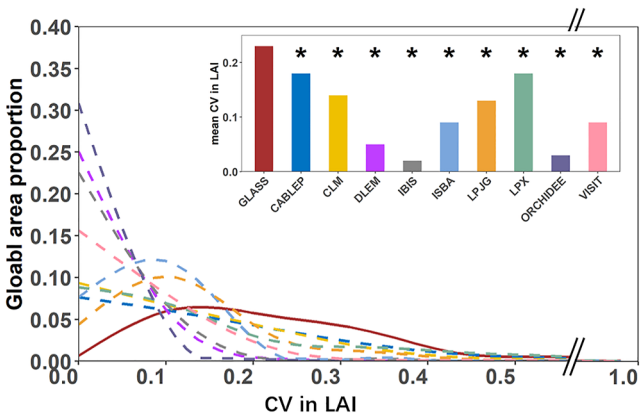

Figure 7. Comparison between the coefficient of variation (CV) of satellite-based leaf area index (LAI) (Global Land Surface Satellite [GLASS]) and simulated LAI by nine terrestrial ecosystem models. *Y*-axis shows area percentage of the corresponding CV in LAI. The inset shows the mean CV of LAI derived from satellite data set and nine ecosystem models. The asterisks (*) indicate the statistically significant differences ($p < 0.05$) between CV in GLASS-LAI and CV in simulated LAI over global vegetated area.

The models predicted lower contributions of canopy physiology on IAV in GPP than observations (Figure 8). Many studies based on observations highlighted the large contributions of physiological changes to IAV in GPP (Messori et al., 2019; Migliavacca et al., 2017; Musavi et al., 2016). Changes in annual GPP because of variations in canopy physiology have been widely reported (Desai, 2010; Zscheischler et al., 2016). A recent study showed a worldwide impact of atmospheric water demand on IAV in GPP by affecting plant stomatal conductance (He et al., 2021). In addition, biotic factors such as plant composition and stand age can also influence IAV in GPP via plant physiology (Polley et al., 2013). For example, Musavi et al. (2017) reported that an increase in stand age and species richness could increase the complementary

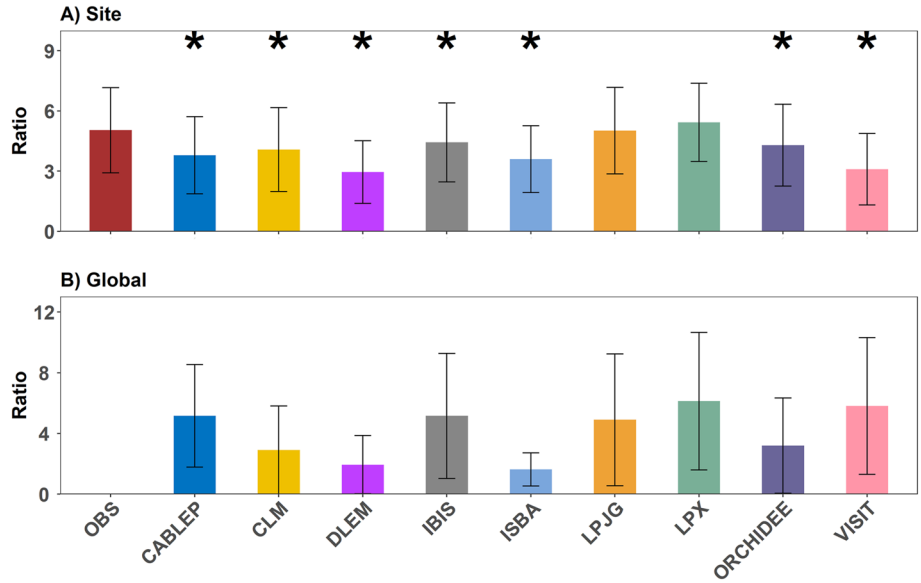

Figure 8. The contribution ratio of physiological and structural changes to interannual variability (IAV) in gross primary production (GPP) averaged at 211 eddy covariance sites (a) and global scale (b). OBS indicates the ratio derived from observations at 211 EC sites. The asterisks (*) indicate statistically significant differences ($p < 0.05$) between model simulation and observation. A higher ratio indicates larger contribution of physiological change to the IAV of GPP. Since there is no globally spatial continuously benchmark of IAV in GPP, the ratio in global observation is absent.

use of nutrients and water, leading to lower IAV in GPP. In summary, our results highlight the importance of reproducing physiological contributions to IAV in GPP (Baldocchi et al., 2018; Keenan et al., 2012).

This study used the coefficient of variance (CV) to indicate IAV in GPP. Standard deviation (SD) and mean value (mean) jointly determine the CV value. This study suggests that the current TEMs underestimate IAV (i.e., lower CV in GPP simulations) (Figure 1), and the lower SD or higher mean of GPP simulations may result in lower CV. Therefore, it is necessary to analyze the dominant cause for underestimating CV. We analyzed the mean magnitude of GPP and LAI for each ecosystem type. Basically, GPP simulations of all TEMs are comparable with the GPP observations (Figure S4 in Supporting Information S1), and over most ecosystem types, the mean values of GPP simulations are lower than observations. This result indicates that a lower SD in the simulation is the main cause for underestimating the CV of GPP, and not the overestimated mean values of GPP.

4.2. Implications of Underestimated GPP Interannual Variability by TEMs

This study highlighted the underestimation of IAV in GPP by the state-of-the-art TEMs, which may result in underestimated IAV in NEP (Yuan et al., 2009). However, recent research showed that the TEMs have good performance of reproducing IAV in NEP at continental scale (Ciais et al., 2019; Piao et al., 2020). NEP is differences between GPP and ecosystem respiration (ER). Therefore, model parameterization is mostly going to improve the model performance for NEP but not GPP or ER, and which is the most important variable because it directly indicates the ecosystem carbon budget. Previous studies have shown that the NEP simulations of various TEMs are quite close, but there are large differences for GPP or ER (Jian et al., 2022; Lu et al., 2021), which implies that the uncertainties in GPP and ER simulations may result in a good performance of NEP. Our study found an underestimation of IAV in GPP by most investigated TEMs, implying that these ecosystem models may have large uncertainty in reproducing IAV in ER. Therefore, it is urgently necessary to investigate the model performance of the IAV in GPP, ER, and NEP.

Our results also showed the larger underestimations of IAV in GPP at nonforest ecosystem types than forest types, especially in arid and semiarid grassland and shrubland (Figures 2 and 3, Figure S1 in Supporting Information S1). A previous study reported that IAV in global carbon sink was driven by gross vegetation production of semiarid lands in the Southern Hemisphere (Poulter et al., 2014). For example, about 80% of the global gross vegetation production anomaly in 2011, an exceptional year with a large land carbon sink, can be explained by only three

main semiarid regions: Australia, temperate South America and southern Africa (Poulter et al., 2014). For arid ecosystems, the water stress is the most important factor for determining the IAV of vegetation growth (Hu et al., 2022). For example, H. J. Xu et al. (2019) reported that summer precipitation primarily controlled the IAV in desert GPP. Therefore, it is important to improve the model performance for reproducing the impacts of water stress on gross vegetation production. On the one hand, the current models need to accurately incorporate the impacts of water stress on vegetation growth processes (Franks et al., 2018). It is also another challenge to represent the diverse responses of vegetation growth to water stress (Grossiord et al., 2020).

4.3. Improvement of TEMs for Simulating Interannual Variability of GPP

There are plenty of methods that may help reproducing IAV in GPP. The most important way is to improve the algorithms for representing environmental regulations of GPP, especially for these environmental variables which highly dominate vegetation growth over large and global scales. Several recent studies highlighted that atmospheric water demand is an important environmental variable for determining global gross vegetation production (He et al., 2021; Lu et al., 2022). For example, from 1982 to 2015, about 70% of the global vegetated area showed a negative correlation of IAV between vegetation growth and atmospheric vapor pressure deficit (VPD) (He et al., 2021). Our study includes nine state-of-the-art TEMs, most of which use physiological-based model to simulate photosynthesis (Farquhar et al., 1980; Haverd et al., 2017; Ito, 2003; Raczka et al., 2021), and two of them (i.e., IBIS, ISBA) use a semi-empirical model (De Pue et al., 2022; Yuan et al., 2014). Although these two types of models incorporate the impacts of VPD on photosynthesis, a recent study showed that these TEMs failed to reproduce the impacts of VPD on gross vegetation production (Yuan et al., 2019). Numerous studies suggested that stomatal conductance declines under high VPD until a given VPD threshold, leading to a cascade of subsequent impacts including photosynthesis reduction, higher risks of carbon starvation and hydraulic failure (Bunce, 2006; Franks et al., 1997). However, there is no consensus on which robust mechanisms drives stomatal closure in response to rising VPD as these mechanisms are varying among environmental gradients and plant functional types (Grossiord et al., 2020). Therefore, the TEMs should better quantify the impact of VPD on stomatal conductance (Franks et al., 2018).

In addition, model-data comparison can play an important role in improving model performance, which may transfer our understandings of the differential changes in photosynthesis response to climate change to improving model predictive skills (Y. Q. Luo et al., 2012). Specifically, to improve models' ability to simulate IAV in GPP, it is urgent to understand the process mechanisms by means of substantial field or laboratory control experiments, underlying the responses of IAV in GPP to environmental changes and comparing the model algorithms with these process-based understandings to improve them accordingly (S. Li et al., 2019; Lu et al., 2021). In addition, there is a need to conduct a data assimilation to further minimize model errors and model-data mismatches. In general, the integration of models, observations, experiments, and process understandings should help improve models' reproduction of IAV in GPP at various scales.

5. Conclusion

In this study, we compared IAV in GPP from the flux tower observations to that from TEM simulations. We found that all the TEMs substantially underestimate the IAV in simulated GPP in comparison to observations, especially in nonforest sites such as grassland and shrubland. There are two main reasons for the underestimation of IAV in GPP from TEMs. On one hand, IAV in canopy structure (i.e., LAI) strongly drives the IAV in GPP from TEMs. However, IAV in model-simulated LAI are much less than them from observations. On the other hand, the TEMs underestimate the changes of canopy physiology response to climate change, resulting in an underestimation of IAV in GPP. Our results suggest that the future versions of TEM to precisely characterize the contribution of canopy physiological changes on the IAV in GPP and clarify the reason for the underestimated variability in LAI. With these efforts, it may be possible to accurately predict the IAV in GPP and the stability of the global carbon sink in the context of global climate change.

Data Availability Statement

The TRENDY v10 ensemble can be accessed with requests from the data hub of the Global Carbon Budget (https://globalcarbonbudgetdata.org/index.html). The GPP data from flux sites are available with requests from FLUXNET2015 data set (https://fluxnet.org/data/fluxnet2015-dataset/), Integrated Carbon Observation System

(ICOS, https://www.icos-cp.eu/data-products/2G60-ZHAK), AmeriFlux (https://ameriflux.lbl.gov/sites/site-search/), OzFlux (https://data.ozflux.org.au/portal/home.jspx), AsiaFlux (https://db.cger.nies.go.jp/asiafluxdb/), and ChinaFLUX (http://www.nesdc.org.cn/theme/index?projectId=612458897e28172cbed3d77a). Some of the data links can be found at the Table S1 in Supporting Information S1. The meteorology data are available at the Climatic Research Unit Japanese Reanalysis (CRU-JRA, http://catalogue.ceda.ac.uk/uuid/863a47a6d-8414b6982e1396c69a9efe8). The GLASS-LAI product is available from the website of GLASS product (http://www.glass.umd.edu/Download.html).

Acknowledgments

This work was supported by the Guangdong Major Project of Basic and Applied Basic Research (2020B0301030004). Shangrong Lin was funded by the National Natural Science Foundation of China, Grant 42101319, the Fundamental Research Funds for the Central Universities, and Sun Yat-sen University (2021qntd29). This work used eddy covariance data acquired and shared by the FLUXNET community, including these networks: AmeriFlux, AfriFlux, AsiaFlux, CarboAfrica, CarboEuropeIP, CarboItaly, CarboMont, ChinaFlux, Fluxnet-Canada, GreenGrass, ICOS, KoFlux, LBA, NECC, OzFlux-TERN, TCOS-Siberia, and USCCC. The FLUXNET eddy covariance data processing and harmonization was carried out by the European Fluxes Database Cluster, AmeriFlux Management Project, and Fluxdata project of FLUXNET, with the support of CDIAC and ICOS Ecosystem Thematic Center, and the OzFlux, ChinaFlux and AsiaFlux offices. We also thank the PIs from global carbon budget project for providing the TRENDY v10 data.

References

Baldocchi, D., Chu, H., & Reichstein, M. (2018). Inter-annual variability of net and gross ecosystem carbon fluxes: A review. *Agricultural and Forest Meteorology*, *249*, 520–533. https://doi.org/10.1016/j.agrformet.2017.05.015

Bastos, A., Ciais, P., Friedlingstein, P., Sitch, S., Pongratz, J., Fan, L., et al. (2020). Direct and seasonal legacy effects of the 2018 heat wave and drought on European ecosystem productivity. *Science advances*, *6*(24), eaba2724. https://doi.org/10.1126/sciadv.aba2724

Beer, C., Reichstein, M., Tomelleri, E., Ciais, P., Jung, M., Carvalhais, N., et al. (2010). Terrestrial gross carbon dioxide uptake: Global distribution and covariation with climate. *Science*, *329*(5993), 834–838. https://doi.org/10.1126/science.1184984

Bertrand, R., Lenoir, J., Piedallu, C., Dillon, G. R., De Ruffray, P., Vidal, C., et al. (2011). Changes in plant community composition lag behind climate warming in lowland forests. *Nature*, *479*(7374), 517–520. https://doi.org/10.1038/nature10548

Bonan, G. B., & Doney, S. C. (2018). Climate, ecosystems, and planetary futures: The challenge to predict life in Earth system models. *Science*, *359*(6375), eaam8328. https://doi.org/10.1126/science.aam8328

Bunce, J. A. (2006). How do leaf hydraulics limit stomatal conductance at high water vapour pressure deficits? *Plant, Cell and Environment*, *29*(8), 1644–1650. https://doi.org/10.1111/j.1365-3040.2006.01541.x

Cai, W., Yuan, W., Liang, S., Liu, S., Dong, W., Chen, Y., et al. (2014). Large differences in terrestrial vegetation production derived from satellite-based light use efficiency models. *Remote Sensing*, *6*(9), 8945–8965. https://doi.org/10.3390/rs6098945

Cao, M., Prince, S. D., Li, K., Tao, B., Small, J., & Shao, X. (2003). Response of terrestrial carbon uptake to climate interannual variability in China. *Global Change Biology*, *9*(4), 536–546. https://doi.org/10.1046/j.1365-2486.2003.00617.x

Chen, J. M., Ju, W., Ciais, P., Viovy, N., Liu, R., Liu, Y., & Lu, X. (2019). Vegetation structural change since 1981 significantly enhanced the terrestrial carbon sink. *Nature Communications*, *10*(1), 4–10. https://doi.org/10.1038/s41467-019-12257-8

Chen, M., Rafique, R., Asrar, G. R., Bond-Lamberty, B., Ciais, P., Zhao, F., et al. (2017). Regional contribution to variability and trends of global gross primary productivity. *Environmental Research Letters*, *12*(10), 105005. https://doi.org/10.1088/1748-9326/aa8978

Chen, S., Zou, J., Hu, Z., & Lu, Y. (2019). Climate and vegetation drivers of terrestrial carbon fluxes: A global data synthesis. *Advances in Atmospheric Sciences*, *36*(7), 679–696. https://doi.org/10.1007/s00376-019-8194-y

Ciais, P., Tan, J., Wang, X., Roedenbeck, C., Chevallier, F., Piao, S. L., et al. (2019). Five decades of northern land carbon uptake revealed by the interhemispheric CO_2 gradient. *Nature*, *568*(7751), 221–225. https://doi.org/10.1038/s41586-019-1078-6

Delire, C., Séférian, R., Decharme, B., Alkama, R., Calvet, J. C., Carrer, D., et al. (2020). The global land carbon cycle simulated with ISBA-CTRIP: Improvements over the last decade. *Journal of Advances in Modeling Earth Systems*, *12*(9), 1–31. https://doi.org/10.1029/2019MS001886

De Pue, J., Barrios, J. M., Liu, L., Ciais, P., Arboleda, A., Hamdi, R., et al. (2022). Local-scale evaluation of the simulated interactions between energy, water and vegetation in ISBA, ORCHIDEE and a diagnostic model. *Biogeosciences*, *19*(17), 4361–4386. https://doi.org/10.5194/bg-19-4361-2022

Desai, A. R. (2010). Climatic and phenological controls on coherent regional interannual variability of carbon dioxide flux in a heterogeneous landscape. *Journal of Geophysical Research*, *115*(4), 1–13. https://doi.org/10.1029/2010JG001423

Desai, A. R., Helliker, B. R., Moorcroft, P. R., Andrews, A. E., & Berry, J. A. (2010). Climatic controls of interannual variability in regional carbon fluxes from top-down and bottom-up perspectives. *Journal of Geophysical Research*, *115*(G2), G02011. https://doi.org/10.1029/2009JG001122

Dietze, M. C., Vargas, R., Richardson, A. D., Stoy, P. C., Barr, A. G., Anderson, R. S., et al. (2011). Characterizing the performance of ecosystem models across time scales: A spectral analysis of the North American carbon program site-level synthesis. *Journal of Geophysical Research*, *116*(4), G04029. https://doi.org/10.1029/2011JG001661

Dong, J., Li, L., Li, Y., & Yu, Q. (2022). Inter-comparisons of mean, trend and interannual variability of global terrestrial gross primary production retrieved from remote sensing approach. *Science of the Total Environment*, *822*, 153343. https://doi.org/10.1016/j.scitotenv.2022.153343

Doughty, R., Köhler, P., Frankenberg, C., Magney, T. S., Xiao, X., Qin, Y., et al. (2019). TROPOMI reveals dry-season increase of solar-induced chlorophyll fluorescence in the Amazon forest. *Proceedings of the National Academy of Sciences of the United States of America*, *116*(44), 22393–22398. https://doi.org/10.1073/pnas.1908157116

Fang, H., Jiang, C., Li, W., Wei, S., Baret, F., Chen, J. M., et al. (2013). Characterization and intercomparison of global moderate resolution leaf area index (LAI) products: Analysis of climatologies and theoretical uncertainties. *Journal of Geophysical Research: Biogeosciences*, *118*(2), 529–548. https://doi.org/10.1002/jgrg.20051

Farquhar, G. D., von Caemmerer, S., & Berry, J. A. (1980). A biochemical model of photosynthetic CO_2 assimilation in leaves of C_3 species. *Planta*, *149*(1), 78–90. https://doi.org/10.1007/BF00386231

Franks, P. J., Bonan, G. B., Berry, J. A., Lombardozzi, D. L., Holbrook, N. M., Herold, N., & Oleson, K. W. (2018). Comparing optimal and empirical stomatal conductance models for application in Earth system models. *Global Change Biology*, *24*(12), 5708–5723. https://doi.org/10.1111/gcb.14445

Franks, P. J., Cowan, I. R., & Farquhar, G. D. (1997). The apparent feedforward response of stomata to air vapour pressure deficit: Information revealed by different experimental procedures with two rainforest trees. *Plant, Cell and Environment*, *20*(1), 142–145. https://doi.org/10.1046/j.1365-3040.1997.d01-14.x

Friedlingstein, P., Jones, M. W., Sullivan, M. O., Andrew, R. M., Bakker, D. C. E., Hauck, J., et al. (2022). Global carbon budget 2021. *Earth System Science Data*, *14*(4), 1917–2005. https://doi.org/10.5194/essd-14-1917-2022

Friedlingstein, P., Sullivan, M. O., Jones, M. W., Andrew, R. M., & Hauck, J. (2020). Global carbon budget 2020. *Earth System Science Data*, *12*(4), 3269–3340. https://doi.org/10.5194/essd-12-3269-2020

Grossiord, C., Grossiord, C., Buckley, T. N., Cernusak, L. A., Novick, K. A., Poulter, B., et al. (2020). Tansley review plant responses to rising vapor pressure deficit. *New Phytologist*, *226*(6), 1550–1566. https://doi.org/10.1111/nph.16485

Haverd, V., Smith, B., Nieradzik, L., Briggs, P., Woodgate, W., Trudinger, C., & Canadell, J. (2017). A new version of the CABLE land surface model (Subversion revision r4546), incorporating land use and land cover change, woody vegetation demography and a novel optimisation-based approach to plant coordination of electron transport and carboxylation capa. *Geoscientific Model Development, ii*, 1–33. https://doi.org/10.5194/gmd-2017-265

He, B., Chen, C., Lin, S., Yuan, W., Chen, H. W., Chen, D., et al. (2021). Worldwide impacts of atmospheric vapor pressure deficit on the interannual variability of terrestrial carbon sinks. *National Science Review*, *9*(4), nwab150. https://doi.org/10.1093/nsr/nwab150

Higuchi, K., Shashkov, A., Chan, D., Saigusa, N., Murayama, S., Yamamoto, S., et al. (2005). Simulations of seasonal and inter-annual variability of gross primary productivity at Takayama with BEPS ecosystem model. *Agricultural and Forest Meteorology*, *134*(1–4), 143–150. https://doi.org/10.1016/j.agrformet.2005.08.018

Hu, Z., Piao, S., Knapp, A. K., Wang, X., Peng, S., Yuan, W., et al. (2022). Decoupling of greenness and gross primary productivity as aridity decreases. *Remote Sensing of Environment*, *279*, 113120. https://doi.org/10.1016/j.rse.2022.113120

Hu, Z., Shi, H., Cheng, K., Wang, Y. P., Piao, S., Li, Y., et al. (2018). Joint structural and physiological control on the interannual variation in productivity in a temperate grassland: A data-model comparison. In *Global change biology* (Vol. 24, No. (7)). https://doi.org/10.1111/gcb.14274

Ito, A. (2003). A global-scale simulation of the CO_2 exchange between the atmosphere and the terrestrial biosphere with a mechanistic model including stable carbon isotopes, 1953–1999. *Tellus B: Chemical and Physical Meteorology*, *55*(2), 596–612. https://doi.org/10.1034/j.1600-0889.2003.01423.x

Jian, J., Bailey, V., Dorheim, K., Konings, A. G., Hao, D., Shiklomanov, A. N., et al. (2022). Historically inconsistent productivity and respiration fluxes in the global terrestrial carbon cycle. *Nature Communications*, *13*(1), 1733. https://doi.org/10.1038/s41467-022-29391-5

Jung, M., Reichstein, M., Schwalm, C. R., Huntingford, C., Sitch, S., Ahlström, A., et al. (2017). Compensatory water effects link yearly global land CO_2 sink changes to temperature. *Nature*, *541*(7638), 516–520. https://doi.org/10.1038/nature20780

Kato, E., Kinoshita, T., Ito, A., Kawamiya, M., & Yamagata, Y. (2013). Evaluation of spatially explicit emission scenario of land-use change and biomass burning using a process-based biogeochemical model. *Journal of Land Use Science*, *8*(1), 104–122. https://doi.org/10.1080/1747423X.2011.628705

Keenan, T. F., Baker, I., Barr, A., Ciais, P., Davis, K., Dietze, M., et al. (2012). Terrestrial biosphere model performance for inter-annual variability of land-atmosphere CO_2 exchange. *Global Change Biology*, *18*(6), 1971–1987. https://doi.org/10.1111/j.1365-2486.2012.02678.x

Lawrence, D. M., Fisher, R. A., Koven, C. D., Oleson, K. W., Swenson, S. C., Bonan, G., et al. (2019). The community land model version 5: Description of new features, benchmarking, and impact of forcing uncertainty. *Journal of Advances in Modeling Earth Systems*, *11*(12), 4245–4287. https://doi.org/10.1029/2018MS001583

Li, S., Yuan, W., Ciais, P., Viovy, N., Ito, A., Jia, B., & Zhu, D. (2019). Benchmark estimates for aboveground litterfall data derived from ecosystem models. *Environmental Research Letters*, *14*(8), 084020. https://doi.org/10.1088/1748-9326/ab2ee4

Li, X., & Xiao, J. (2020). Agricultural and Forest Meteorology Global climatic controls on interannual variability of ecosystem productivity: Similarities and differences inferred from solar-induced chlorophyll fluorescence and enhanced vegetation index. *Agricultural and Forest Meteorology*, *288–289*, 108018. https://doi.org/10.1016/j.agrformet.2020.108018

Li, Z., Ahlström, A., Tian, F., Gärtner, A., Jiang, M., & Xia, J. (2020). Minimum carbon uptake controls the interannual variability of ecosystem productivity in tropical evergreen forests. *Global and Planetary Change*, *195*, 103343. https://doi.org/10.1016/j.gloplacha.2020.103343

Liang, S., Cheng, J., Jia, K., Jiang, B., Liu, Q., Xiao, Z., et al. (2021). The global land surface satellite (GLASS) product suite. *Bulletin of the American Meteorological Society*, *102*(2), E323–E337. https://doi.org/10.1175/BAMS-D-18-0341.1

Liaw, A., & Wiener, M. (2002). Classification and regression by randomForest. *R News*, *2*(3), 18–22. Retrieved from https://cran.r-project.org/doc/Rnews/

Lienert, S., & Joos, F. (2018). A Bayesian ensemble data assimilation to constrain model parameters and land-use carbon emissions. *Biogeosciences*, *15*(9), 2909–2930. https://doi.org/10.5194/bg-15-2909-2018

Liu, F., Wang, X., Wang, C., & Zhang, Q. (2021). Environmental and biotic controls on the interannual variations in CO_2 fluxes of a continental monsoon temperate forest. *Agricultural and Forest Meteorology*, *296*, 108232. https://doi.org/10.1016/j.agrformet.2020.108232

Lu, H., Li, S., Ma, M., Bastrikov, V., Chen, X., Ciais, P., et al. (2021). Comparing machine learning-derived global estimates of soil respiration and its components with those from terrestrial ecosystem models. *Environmental Research Letters*, *16*(5), 054048. https://doi.org/10.1088/1748-9326/abf526

Lu, H., Qin, Z., Lin, S., Chen, X., Chen, B., He, B., et al. (2022). Large influence of atmospheric vapor pressure deficit on ecosystem production efficiency. *Nature Communications*, *13*(1), 1–5. https://doi.org/10.1038/s41467-022-29009-w

Luo, X., Keenan, T. F., Croft, H., Chen, J. M., & He, L. (2019). Improved estimates of global terrestrial photosynthesis using information on leaf chlorophyll content. *February*, *25*(7), 2499–2514. https://doi.org/10.1111/gcb.14624

Luo, Y. Q., Randerson, J. T., Abramowitz, G., Bacour, C., Blyth, E., Carvalhais, N., et al. (2012). A framework for benchmarking land models. *Biogeosciences*, *9*(10), 3857–3874. https://doi.org/10.5194/bg-9-3857-2012

MacBean, N., Maignan, F., Bacour, C., Lewis, P., Peylin, P., Guanter, L., et al. (2018). Strong constraint on modelled global carbon uptake using solar-induced chlorophyll fluorescence data. *Scientific Reports*, *8*(1), 1973. https://doi.org/10.1038/s41598-018-20024-w

Magney, T. S., Bowling, D. R., Logan, B. A., Grossmann, K., Stutz, J., & Blanken, P. D. (2019). Mechanistic evidence for tracking the seasonality of photosynthesis with solar-induced fluorescence. *Proceedings of the National Academy of Sciences of the United States of America*, *116*(24), 11640–11645. https://doi.org/10.1073/pnas.1900278116

Messori, G., Ruiz-Pérez, G., Manzoni, S., & Vico, G. (2019). Climate drivers of the terrestrial carbon cycle variability in Europe. *Environmental Research Letters*, *14*(6), 063001. https://doi.org/10.1088/1748-9326/ab1ac0

Migliavacca, M., Perez-priego, O., Rossini, M., El-madany, T. S., Moreno, G., Van der Tol, C., et al. (2017). Plant functional traits and canopy structure control the relationship between photosynthetic CO_2 uptake and far-red sun-induced fluorescence in a Mediterranean grassland under different nutrient availability. *New Phytologist*, *214*(3), 1078–1091. https://doi.org/10.1111/nph.14437

Mulder, C. P. H., Iles, D. T., & Rockwell, R. F. (2017). Increased variance in temperature and lag effects alter phenological responses to rapid warming in a subarctic plant community. *Global Change Biology*, *23*(2), 801–814. https://doi.org/10.1111/gcb.13386

Musavi, T., Migliavacca, M., Reichstein, M., Kattge, J., Wirth, C., Black, T. A., et al. (2017). Stand age and species richness dampen interannual variation of ecosystem-level photosynthetic capacity. *Nature Ecology and Evolution*, *1*(2), 1–6. https://doi.org/10.1038/s41559-016-0048

Musavi, T., Migliavacca, M., van de Weg, M. J., Kattge, J., Wohlfahrt, G., van Bodegom, P. M., et al. (2016). Potential and limitations of inferring ecosystem photosynthetic capacity from leaf functional traits. *Ecology and Evolution*, *6*(20), 7352–7366. https://doi.org/10.1002/ece3.2479

O'Sullivan, M., Smith, W. K., Sitch, S., Friedlingstein, P., Arora, V. K., Haverd, V., et al. (2020). Climate-driven variability and trends in plant productivity over recent decades based on three global products. *Global Biogeochemical Cycles*, *34*(12), e2020GB006613. https://doi.org/10.1029/2020GB006613

Pastorello, G., Trotta, C., Canfora, E., Chu, H., Christianson, D., Cheah, Y. W., et al. (2020). The FLUXNET2015 dataset and the ONEFlux processing pipeline for eddy covariance data. *Scientific Data*, *7*(1), 225. https://doi.org/10.1038/s41597-020-0534-3

Peng, Y., Bloomfield, K. J., Cernusak, L. A., Domingues, T. F., & Colin Prentice, I. (2021). Global climate and nutrient controls of photosynthetic capacity. *Communications Biology*, *4*(1), 1–9. https://doi.org/10.1038/s42003-021-01985-7

Piao, S., Wang, X., Wang, K., Li, X., Sitch, S., Bastos, A., et al. (2020). Interannual variation of terrestrial carbon cycle: Issues and perspectives. *Global Change Biology*, *26*(7543), 300–318. https://doi.org/10.1111/gcb.14884

Polley, H. W., Isbell, F. I., & Wilsey, B. J. (2013). Plant functional traits improve diversity-based predictions of temporal stability of grassland productivity. *Oikos*, *122*(9), 1275–1282. https://doi.org/10.1111/j.1600-0706.2013.00338.x

Poulter, B., Frank, D., Ciais, P., Myneni, R. B., Andela, N., Bi, J., et al. (2014). Contribution of semi-arid ecosystems to interannual variability of the global carbon cycle. *Nature*, *509*(7502), 600–603. https://doi.org/10.1038/nature13376

Raczka, B., Hoar, T. J., Duarte, H. F., Fox, A. M., Anderson, J. L., Bowling, D. R., & Lin, J. C. (2021). Improving CLM5.0 biomass and carbon exchange across the western United States using a data assimilation system. *Journal of Advances in Modeling Earth Systems*, *13*(7), 1–23. https://doi.org/10.1029/2020MS002421

Reichstein, M., Bahn, M., Ciais, P., Frank, D., Mahecha, M. D., Seneviratne, S. I., et al. (2013). Climate extremes and the carbon cycle. *Nature*, *500*(7462), 287–295. https://doi.org/10.1038/nature12350

Saleska, S. R., Wu, J., Guan, K., Araujo, A. C., Huete, A., Nobre, A. D., & Restrepo-Coupe, N. (2016). Dry-season greening of Amazon forests. *Nature*, *531*(7594), E4–E5. https://doi.org/10.1038/nature16457

Seneviratne, S. I., Nicholls, N., Easterling, D., Goodess, C. M., Kanae, S., Kossin, J., et al. (2012). Changes in climate extremes and their impacts on the natural physical environment. *Managing the Risks of Extreme Events and Disasters to Advance Climate Change Adaptation: Special Report of the Intergovernmental Panel on Climate Change*, *9781107025*, 109–230. https://doi.org/10.1017/CBO9781139177245.006

Sherry, R. A., Weng, E., Arnone, J. A., Johnson, D. W., Schimel, D. S., Verburg, P. S., et al. (2008). Lagged effects of experimental warming and doubled precipitation on annual and seasonal aboveground biomass production in a tallgrass prairie. *Global Change Biology*, *14*(12), 2923–2936. https://doi.org/10.1111/j.1365-2486.2008.01703.x

Smith, B., Wärlind, D., Arneth, A., Hickler, T., Leadley, P., Siltberg, J., & Zaehle, S. (2014). Implications of incorporating N cycling and N limitations on primary production in an individual-based dynamic vegetation model. *Biogeosciences*, *11*(7), 2027–2054. https://doi.org/10.5194/bg-11-2027-2014

Stocker, B. D., Zscheischler, J., Keenan, T. F., Prentice, I. C., Seneviratne, S. I., & Peñuelas, J. (2019). Drought impacts on terrestrial primary production underestimated by satellite monitoring. *Nature Geoscience*, *12*, 264–270. https://doi.org/10.1038/s41561-019-0318-6

Tian, H., Chen, G., Lu, C., Xu, X., Hayes, D. J., Ren, W., et al. (2015). North American terrestrial CO_2 uptake largely offset by CH_4 and N_2O emissions: Toward a full accounting of the greenhouse gas budget. *Climatic Change*, *129*(3–4), 413–426. https://doi.org/10.1007/s10584-014-1072-9

Verma, M., Friedl, M. A., Law, B. E., Bonal, D., Kiely, G., Black, T. A., et al. (2015). Improving the performance of remote sensing models for capturing intra- and inter-annual variations in daily GPP: An analysis using global FLUXNET tower data. *Agricultural and Forest Meteorology*, *214–215*, 416–429. https://doi.org/10.1016/j.agrformet.2015.09.005

Vuichard, N., Messina, P., Luyssaert, S., Guenet, B., Zaehle, S., Ghattas, J., et al. (2019). Accounting for carbon and nitrogen interactions in the global terrestrial ecosystem model ORCHIDEE (trunk version, rev 4999): Multi-scale evaluation of gross primary production. *Geoscientific Model Development*, *12*(11), 4751–4779. https://doi.org/10.5194/gmd-12-4751-2019

Walther, S., Voigt, M., Thum, T., Gonsamo, A., Zhang, Y., Köhler, P., et al. (2016). Satellite chlorophyll fluorescence measurements reveal large-scale decoupling of photosynthesis and greenness dynamics in boreal evergreen forests. *Global Change Biology*, *22*(9), 2979–2996. https://doi.org/10.1111/gcb.13200

Wang, W., Dungan, J., Hashimoto, H., Michaelis, A. R., Milesi, C., Ichii, K., & Nemani, R. R. (2011). Diagnosing and assessing uncertainties of terrestrial ecosystem models in a multimodel ensemble experiment: 1. Primary production. *Global Change Biology*, *17*(3), 1350–1366. https://doi.org/10.1111/j.1365-2486.2010.02309.x

Wen, Y., Liu, X., Xin, Q., Wu, J., Xu, X., Pei, F., et al. (2019). Cumulative effects of climatic factors on terrestrial vegetation growth. *Journal of Geophysical Research: Biogeosciences*, *124*(4), 789–806. https://doi.org/10.1029/2018JG004751

Winkler, A. J., Myneni, R. B., Alexandrov, G. A., & Brovkin, V. (2019). Earth system models underestimate carbon fixation by plants in the high latitudes. *Nature Communications*, *10*(1), 885. https://doi.org/10.1038/s41467-019-08633-z

Wu, J., Guan, K., Hayek, M., Restrepo-Coupe, N., Wiedemann, K. T., Xu, X., et al. (2017). Partitioning controls on Amazon forest photosynthesis between environmental and biotic factors at hourly to interannual timescales. *Global Change Biology*, *23*(3), 1240–1257. https://doi.org/10.1111/gcb.13509

Xia, J., Niu, S., Ciais, P., Janssens, I. A., Chen, J., Ammann, C., et al. (2015). Joint control of terrestrial gross primary productivity by plant phenology and physiology. *Proceedings of the National Academy of Sciences of the United States of America*, *112*(9), 2788–2793. https://doi.org/10.1073/pnas.1413090112

Xiao, Z., Liang, S., & Jiang, B. (2017). Evaluation of four long time-series global leaf area index products. *Agricultural and Forest Meteorology*, *246*, 218–230. https://doi.org/10.1016/j.agrformet.2017.06.016

Xiao, Z., Liang, S., Wang, J., Chen, P., Yin, X., Zhang, L., & Song, J. (2014). Use of general regression neural networks for generating the GLASS leaf area index product from time-series MODIS surface reflectance. *IEEE Transactions on Geoscience and Remote Sensing*, *52*(1), 209–223. https://doi.org/10.1109/TGRS.2013.2237780

Xu, B., Li, J., Park, T., Liu, Q., Zeng, Y., Yin, G., et al. (2018). An integrated method for validating long-term leaf area index products using global networks of site-based measurements. *Remote Sensing of Environment*, *209*, 134–151. https://doi.org/10.1016/j.rse.2018.02.049

Xu, H. J., Zhao, C. Y., & Wang, X. P. (2019). Spatiotemporal differentiation of the terrestrial gross primary production response to climate constraints in a dryland mountain ecosystem of northwestern China. *Agricultural and Forest Meteorology*, *276–277*, 107628. https://doi.org/10.1016/j.agrformet.2019.107628

Yuan, W., Liu, D., Dong, W., Liu, S., Zhou, G., Yu, G., et al. (2014). Multiyear precipitation reduction strongly decreases carbon uptake over northern China. *Journal of Geophysical Research: Biogeosciences*, *119*(5), 881–896. https://doi.org/10.1002/2014JG002608

Yuan, W., Luo, Y., Richardson, A. D., Oren, R., Luyssaert, S., Janssens, I. A., et al. (2009). Latitudinal patterns of magnitude and interannual variability in net ecosystem exchange regulated by biological and environmental variables. *Global Change Biology*, *15*(12), 2905–2920. https://doi.org/10.1111/j.1365-2486.2009.01870.x

Yuan, W., Zheng, Y., Piao, S., Ciais, P., Lombardozzi, D., Wang, Y., et al. (2019). Increased atmospheric vapor pressure deficit reduces global vegetation growth. *Science Advances*, *5*(8), eaax1396. https://doi.org/10.1126/sciadv.aax1396

Zhang, Y., Dannenberg, M. P., Hwang, T., & Song, C. (2019). El Niño-Southern Oscillation-induced variability of terrestrial gross primary production during the satellite era. *Journal of Geophysical Research: Biogeosciences*, *124*(8), 2419–2431. https://doi.org/10.1029/2019JG005117

Zhang, Y., & Ye, A. (2021). Would the obtainable gross primary productivity (GPP) products stand up? A critical assessment of 45 global GPP products. *Science of the Total Environment*, *783*, 146965. https://doi.org/10.1016/j.scitotenv.2021.146965

Zhao, A., Yu, Q., Feng, L., Zhang, A., & Pei, T. (2020). Evaluating the cumulative and time-lag effects of drought on grassland vegetation: A case study in the Chinese Loess Plateau. *Journal of Environmental Management*, *261*, 110214. https://doi.org/10.1016/j.jenvman.2020.110214

Zhao, Q., Zhu, Z., Zeng, H., Zhao, W., & Myneni, R. B. (2020). Agricultural and forest meteorology future greening of the Earth may not be as large as previously predicted. *Agricultural and Forest Meteorology*, *292–293*, 108111. https://doi.org/10.1016/j.agrformet.2020.108111

Zheng, Y., Shen, R., Wang, Y., Li, X., Liu, S., Liang, S., et al. (2020). Improved estimate of global gross primary production for reproducing its long-term variation, 1982–2017. *Earth System Science Data*, *12*(4), 2725–2746. https://doi.org/10.5194/essd-12-2725-2020

Zscheischler, J., Fatichi, S., Wolf, S., Blanken, P. D., Bohrer, G., Clark, K., et al. (2016). Short-term favorable weather conditions are an important control of interannual variability in carbon and water fluxes. *Journal of Geophysical Research: Biogeosciences*, *121*(8), 2186–2198. https://doi.org/10.1002/2016JG003503

Zscheischler, J., Mahecha, M. D., Von Buttlar, J., Harmeling, S., Jung, M., Rammig, A., et al. (2014). A few extreme events dominate global interannual variability in gross primary production. *Environmental Research Letters*, *9*(3), 035001. https://doi.org/10.1088/1748-9326/9/3/035001

Zscheischler, J., Michalak, A. M., Schwalm, C., Mahecha, M. D., Huntzinger, D. N., Reichstein, M., et al. (2014). Impact of large-scale climate extremes on biospheric carbon fluxes: An intercomparison based on MsTMIP data. *Global Biogeochemical Cycles*, *28*(6), 585–600. https://doi.org/10.1002/2014GB004826